Local and regional controls on Holocene sea ice dynamics and oceanography in Nares Strait, Northwest Greenland

Eleanor Georgiadis, Jacques Giraudeau, Anne Jennings, Audrey Limoges, Rebecca Jackson, Sofia Ribeiro, Guillaume Massé

Local and regional controls on Holocene sea ice dynamics and oceanography in Nares Strait, Northwest Greenland

Article *in* Marine Geology · April 2020

DOI: 10.1016/j.margeo.2020.106115

CITATIONS
3

READS
108

7 authors, including:

Eleanor Georgiadis
University of Bordeaux
6 PUBLICATIONS **24** CITATIONS
SEE PROFILE

Jacques Giraudeau
French National Centre for Scientific Research
146 PUBLICATIONS **2,909** CITATIONS
SEE PROFILE

Anne E Jennings
University of Colorado Boulder
203 PUBLICATIONS **10,050** CITATIONS
SEE PROFILE

Audrey Limoges
University of New Brunswick
31 PUBLICATIONS **554** CITATIONS
SEE PROFILE

Marine Geology 422 (2020) 106115

Contents lists available at ScienceDirect

Marine Geology

journal homepage: www.elsevier.com/locate/margo

Local and regional controls on Holocene sea ice dynamics and oceanography in Nares Strait, Northwest Greenland

Eleanor Georgiadis[a,b,*], Jacques Giraudeau[a], Anne Jennings[c], Audrey Limoges[d], Rebecca Jackson[e], Sofia Ribeiro[e], Guillaume Massé[b,f]

[a] Université de Bordeaux, CNRS, UMR 5805 EPOC, allée Geoffroy St-Hilaire, 33615 Pessac, France
[b] Université Laval, UMI 3376 TAKUVIK, 1045 avenue de la Médecine, G1V 0A6, Québec, QC, Canada
[c] INSTAAR, University of Colorado, Boulder, CO 80309-0450, USA
[d] Department of Earth Sciences, University of New Brunswick, 2 Bailey Drive, Fredericton, E3B 5A3, Canada
[e] Department of Glaciology and Climate, Geological Survey of Denmark and Greenland, Øster Voldgade 10, Copenhagen 1350, Denmark
[f] Université Sorbonne, CNRS, UMR 7159 LOCEAN, 4 place Jussieu, 7500 Paris Cedex, France

ARTICLE INFO

Editor: Shu Gao

Keywords:
Arctic Ocean and adjacent high latitudes
Paleoceanography
Micropaleontology (forams)
Sea-ice biomarkers
Glacial sediments

ABSTRACT

Nares Strait is one of three channels that connect the Arctic Ocean to Baffin Bay. Unique sea-ice conditions in the strait lead to the formation of landfast ice arches at its northern and southern ends. These ice arches regulate Arctic sea-ice and freshwater export through the strait and promote the opening of the North Water polynya. The present study addresses the paucity of pre-satellite records of environmental conditions in the Nares Strait area, and aims at reconstructing Holocene sea-ice conditions and ocean circulation in the strait. The investigation is based on a marine sediment core strategically retrieved from under the current ice arch in Kane Basin to the south of Nares Strait, and provides a continuous record spanning the past *ca* 9 kyrs. We use benthic foraminiferal assemblages and sea-ice biomarkers to infer changes in Holocene ocean circulation and sea-ice conditions in Kane Basin. The establishment of the modern ocean circulation in Kane Basin is related to ice sheet retreat and postglacial rebound, while changes in sea-ice cover concur with major shifts in the Arctic Oscillation (AO). Our results suggest that sea-ice cover in Kane Basin was highly variable between *ca* 9.0 and 8.3 cal. ka BP, before increasing, probably in link with the 8.2 cold event and the opening of Nares Strait. A short period of minimum sea-ice cover and maximum Atlantic bottom water influence occurred between *ca* 8.1 and 7.5 cal. ka BP, when Kane Basin was deeper than for the remaining of the Holocene. As atmospheric temperatures dropped, sea-ice cover intensified in Kane Basin between *ca* 7.5 and 5.5 cal. ka BP, but strong winds under prevailing positive-like AO conditions likely prevented the formation of ice arches in Nares Strait. During this time, our micropaleontological data show that Atlantic water was progressively excluded from Kane Basin by the postglacial isostatic rebound. Increasingly cooler atmospheric temperatures and a shift towards more negative phases of the AO may have promoted the establishment of ice arches in Nares Strait between *ca* 5.5 and 3.0 cal. ka BP. Instabilities in the Kane Basin ice arch *ca* 3.0 cal. ka BP coincide with a shift towards prevailing positive phases of the AO, while a brief recovery of the ice arch occurred during more negative-like AO conditions between *ca* 1.2 and 0.2 cal. ka BP.

1. Introduction

Nares Strait, located between Greenland and Ellesmere Island, is one of three channels of the Canadian Arctic Archipelago (CAA) linking the Arctic Ocean to Baffin Bay (Fig. 1). The strait is an important gateway for the export of water and sea ice from the Arctic Ocean towards the Atlantic Ocean, contributing to up to half of the volume of water transported through the CAA (McGeehan and Maslowski, 2012). The CAA is a major provider of freshwater to the Labrador Sea where it may influence deep water formation (Belkin et al., 1998). Regional ocean surface dynamics are partly regulated by the unique sea-ice conditions in the strait. The export of Arctic sea ice through Nares Strait ceases annually in the winter and spring, when landfast ice covers the strait, and forms the Kane Basin ice arch (Fig. 1c; Barber et al., 2001). Fresh surface water export through Nares Strait is also reduced in the presence of this ice arch (Münchow, 2016). Furthermore, the Kane

* Corresponding author at: Université de Bordeaux, CNRS, UMR 5805 EPOC, allée Geoffroy St-Hilaire, 33615 Pessac, France.
E-mail address: eleanor.georgiadis@u-bordeaux.fr (E. Georgiadis).

https://doi.org/10.1016/j.margeo.2020.106115
Received 4 October 2019; Received in revised form 21 December 2019; Accepted 25 December 2019
Available online 13 January 2020

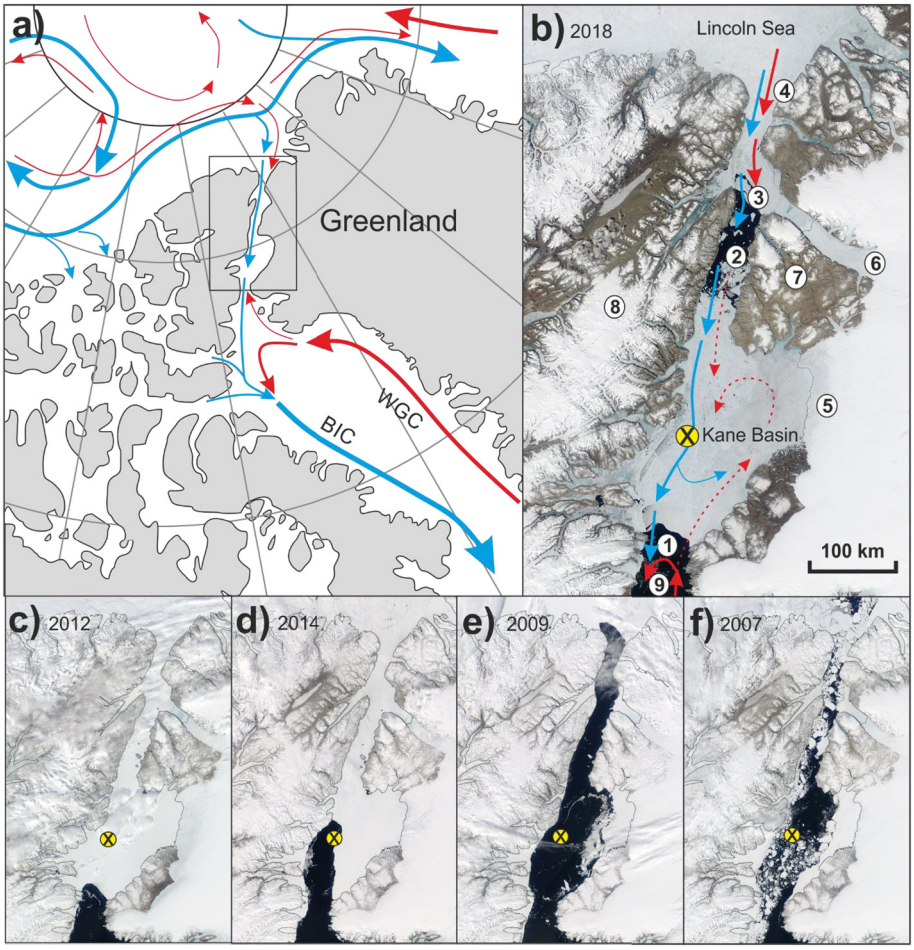

Fig. 1. Schematic circulation in the Canadian and northern Greenland sectors of the Arctic Ocean and Baffin Bay (a) and within Nares Strait (b, snapshot from July 28th 2018), and inter-annual variations in sea ice cover in Nares Strait (c–f). The location of core AMD14-Kane2b is marked by a cross. Blue arrows represent Arctic (surface) water and red arrows deeper Atlantic water, red dashed arrows represent the potential circulation of Atlantic water in Nares Strait. WGC: West Greenland Current, BIC: Baffin Island Current. 1 – Smith Sound; 2 – Kennedy Channel; 3 – Hall Basin; 4 – Robeson Channel; 5 – Humboldt Glacier; 6 – Petermann Glacier; 7 – Washington Land; 8 – Agassiz Ice Cap; 9 – NOW polynya. Snapshots of satellite images from MODIS (500 m resolution) of Nares Strait during the first week of June in: c) 2012 ("typical" location of the southern ice arch), d) 2014 (northern migration of the southern ice arch – the NOW polynya extends to the core site), e) 2009 (northern ice arch in the Lincoln Sea – the southern ice arch failed to form), and f) 2007 (year-round throughflow of ice – both ice arches failed to form). Satellite image source: https://worldview.earthdata.nasa.gov/. (For interpretation of the references to colour in this figure legend, the reader is referred to the web version of this article.)

Basin ice arch is integral in maintaining the North Water (NOW polynya; Fig. 1b), as it prevents sea ice and icebergs from drifting into northern Baffin Bay, while northerly winds and ocean currents sweep away any newly formed sea-ice in the polynya (Melling et al., 2001). The Kane Basin ice arch is formed by the congestion of multi-year sea ice from the Arctic Ocean and glacial ice calved from the Petermann and Humboldt Glaciers (Fig. 1b). The particular morphology of the strait promotes the build-up of ice in the southern part of the strait as (1) an anti-cyclonic gyre in the wider Kane Basin can slowdown and trap drift ice and icebergs (Nutt, 1966), and (2) the coastline forms a bottleneck on either side of Smith Sound and restricts the southern exit of Kane Basin. Another ice arch occasionally forms to the north of the strait along the Robeson Channel (Fig. 1e) by the convergence of thick multi-year ice in the Lincoln Sea (Kwok et al., 2010). A polynya in the south of the Lincoln Sea and in northern Nares Strait can be promoted by this northern ice arch, but it has been less studied than its southern counterpart (Kozo, 1991). Simulations have shown that the thickness of the ice forming these arches is a key factor in determining their resistance to the strong winds in Nares Strait (Dumont et al., 2009), suggesting that ice arch break-up is at least partly dictated by the effect of wind stress on thinning ice during the spring or summer. Locally, winds are orographically channelled by the steep coastal topography of Nares Strait, and their strength is correlated to the sea level pressure difference between northern and southern Nares Strait (Samelson and Barbour, 2008). While winds play a role in the predominantly southward flowing ocean surface current in Nares Strait, the main driver of this flow is considered to be the sea level difference between the Lincoln Sea and Baffin Bay (Münchow and Melling, 2008). The ingress of the West Greenland Current (WGC) into southern Nares Strait constitutes a counter-current of northward Atlantic-sourced water that runs through Smith Sound (Fig. 1b; Münchow et al., 2007), but the extent of its reach into Kane Basin is unclear. The water column in Nares Strait is stratified, with southward Arctic and Pacific water carried in the top 50 m, and a mix of Atlantic and Pacific water below this depth (Jones and Eert, 2004; Münchow et al., 2007). Most of the Atlantic water in Kane Basin is considered to enter via the north, from the Arctic Ocean (e.g. Münchow et al., 2011), although some may enter via the south, from Baffin Bay, in varying amounts (e.g. Sadler, 1976).

Nares Strait has been the focus of a number of short-lived monitoring programs, and concerns have been raised regarding the future of the ice arches in the context of global warming. Some of the first documented observations of the NOW polynya in the literature report that the breakup of the southern ice arch usually occurred in late July or August in the 1960s, and as late as mid-August in 1967 (Dunbar, 1969). In the late 1990s and early 2000s, the ice arches typically collapsed in early July (Kwok et al., 2010). In the winter of 2006–2007, both ice arches failed to form for the first time in the satellite era (Kwok et al., 2010). Since then, a trend of late formation, early breakup or complete failure to form has been observed (Moore and McNeil, 2018; Münchow, 2016), and is associated with decreasing primary productivity in the NOW polynya (Marchese et al., 2017). Those recent observations may suggest that the area is currently witnessing a rapid transition in sea ice dynamics (Moore and McNeil, 2018).

Long-term perspectives on sea-ice dynamics in Nares Strait are essential to better understand their response to climatic forcing. Such records extending beyond the satellite era are however scarce in Nares Strait. Here, we present the first reconstruction of sea-ice cover and oceanographic circulation in Kane Basin, based on the study of a 4.25 m long marine sediment core (AMD14-Kane2b) strategically retrieved from under the current southern ice arch that provides a continuous

record of the past *ca* 9 cal. ka BP.

Nares Strait is situated along the former confluence of the Innuitian Ice Sheet (IIS) and the Greenland Ice Sheet (GIS), and was covered by glacial ice until *ca* 9–8 cal. ka BP (e.g. England, 1999; Georgiadis et al., 2018; Jennings et al., 2011, 2019). In addition to the drastic climatic shift during the deglaciation (*ca* 18–8 cal. ka BP), Nares Strait has undergone a major spatial reorganisation associated with ice sheet retreat and postglacial isostatic rebound during the Holocene (11.7–0 cal. ka BP). The opening of the Nares Strait also established a direct atmospheric channel between the polar vortex and Baffin Bay.

In this paper, we aspire to (1) reconstruct the Holocene environmental evolution of Kane Basin based on benthic foraminiferal assemblages and sea-ice biomarkers (IP_{25} and HBI III), and (2) establish possible links between sea-ice dynamics and ocean circulation in the strait with local (geomorphologic) and regional (climatic) forcing. This work builds-on a previous sedimentological and geochemical study on the same core which laid the foundations for the post-glacial history of Nares Strait (Georgiadis et al., 2018).

2. Material and methods

2.1. Sediment core AMD14-Kane2b

The 4.25 m long marine sediment core AMD14-Kane2b (79°30′ N 70°51′ W, 220 m water depth) was retrieved in Kane Basin, the central basin of Nares Strait, with a CASQ – Calypso Square – corer during the 2014 ArcticNet cruise of CCGS *Amundsen*. A full description of sediment facies for this record is given in Georgiadis et al. (2018). Of particular interest are two units which are rich in ice-rafted debris (IRD) in the bottom half of the core dated at *ca* 9.0 cal. ka BP and 8.3 cal. ka BP, both of which fall within the time frame of the collapse of the glacial buttress in Kennedy Channel based on previous datings of the event (England, 1999; Jennings et al., 2011, 2019). Georgiadis et al. (2018) argued that these lithofacies were likely linked to (1) a retreating ice-marginal environment *ca* 9 cal. ka BP, and (2) the collapse of the glacial buttress in Kennedy Channel which established the connection of the Arctic Ocean to Baffin Bay through Nares Strait *ca* 8.3 cal. ka BP.

The age model of core AMD14-Kane2b is presented in Caron et al., 2019 and Georgiadis et al. (2018). It is based on 14 AMS radiocarbon ages measured on benthic foraminifera and mollusc shells and corrected with $\Delta R = 240 \pm 55$ years. Sedimentation rates decrease from ~220 $cm.ka^{-1}$ at the very base of the core to ~30–50 $cm.ka^{-1}$ in the remaining 3.5 m of the core. ^{210}Pb measurements indicate that the core recovered modern sediments and suggests an average age for the core top of ~60 years (1955 CE) with low sedimentation rates of ~20 $cm.ka^{-1}$.

2.2. Sea-ice biomarkers

The sea-ice biomarkers used in this study are the Highly Branched Isoprenoids (HBI) IP_{25} (Ice Proxy with 25 atoms of carbon) and HBI III (tri-unsaturated HBI). Their abundances were determined at a 1 to 4 cm resolution (10–160 years according to our age model) and following the protocol described by Belt and Müller (2013). Concentrations of IP_{25} and HBI III are expressed in $ng{\cdot}g^{-1}$ of dry sediment. In the absence of a pure HBI III standard, the concentrations of this biomarker are expressed in $ng{\cdot}g^{-1}$ of internal standard equivalent.

Biomarker fluxes (concentration*density*sedimentation rate) were calculated using the CT-number as a proxy for sediment density, and are thus expressed in number/unit surface area/year (for additional information, please refer to Georgiadis et al., 2018).

IP_{25} is synthesised by spring, and, to a minor extent, summer sea-ice dwelling diatoms *Haslea spicula*, *H. kjellmanii* and *Pleurosigma stuxbergii* var. *rhomboides* (Brown et al., 2014). IP_{25} is considered as a proxy for seasonal sea-ice cover. Its absence in sediment indicates either year-round ice-free (absence of habitat for sea-ice diatoms) or permanently ice-covered (absence of detachment of the ice algae, and/or potential light limitation) waters (Belt and Müller, 2013). Freshwater input in coastal Arctic settings has been identified as being potentially detrimental to IP_{25} production in sea ice, and changes in salinity should not be overlooked as a source of IP_{25} variability (Ribeiro et al., 2017). HBI III has been found to be synthetized by the two sea-ice margin diatom genera *Pleurosigma* and *Rhizosolenia* (Belt et al., 2010) generally associated with planktic ice-edge productivity and freshwater (Ribeiro et al., 2017).

The spatial variability of IP_{25} and HBI III concentrations in Arctic regions causes difficulties in converting given biomarker concentrations into quantitative sea ice reconstructions. Biomarker abundances have been used in paleoceanographic studies as a means of reconstructing the changes in sea-ice dynamics by observing the relative variations of biomarkers through time at a given location (e.g. Belt et al., 2010). Although in situ HBI measurements have not yet been carried out in Nares Strait, we assume that HBI III-producing diatoms may dwell in the ice-packed, fresher surface water following ice arch break-up. The irregular under-ice environment of the Kane Basin ice arch – made up of varying amounts of thick multi-year ice consolidated by thinner first year ice – and the continuous supply of nutrients by the throughflow of Pacific-sourced Arctic water constitutes an ideal environment for IP_{25}-producing sea-ice algae (Krembs et al., 2002).

2.3. Foraminifera

One centimeter-thick slices of approximately 25 cm^3 of sediment were sampled and dried before wet sieving through 63 and 125 μm meshes. Benthic and planktic foraminifera census counts were performed on the oven-dried residue of each fraction every 4–16 cm throughout the core. This protocol (drying before and after sieving, and dry counting) has been a standard practice in micropaleontological studies including those conducted on marine sediments from the High Arctic, but this method is no longer recommended due to the loss of poorly cemented agglutinated and more fragile calcareous species (Sperling et al., 2002). Our foraminiferal assemblages were however diverse, and dominant taxa were similar to those found in nearby micropaleontological studies (Jennings et al., 2019; Knudsen et al., 2008). Concentrations of benthic and planktic foraminifera are expressed in number of individuals per gram of dry sediment, and fluxes (concentrations*density*sedimentation rates) are expressed in an arbitrary unit of number of individuals/unit surface area/year.

Foraminiferal assemblages offer detailed insight regarding past marine environmental conditions owing to the fossilisation potential of foraminifera tests and specific environmental preferences. Such information as the abundance of food supply, the occurrence of sea ice cover, and the presence of Atlantic water at the bottom can be provided by the specific composition of the assemblages.

A stratigraphically constrained cluster analysis (CONISS, Grimm, 1987) was performed on the relative abundance of calcareous benthic species using the vegan (Oksanen et al., 2019), mgcv (Wood, 2019) and grDevices (R Core Team, 2017) packages in R. The data and ecozones (i.e. clusters) were plotted using the Rioja package in R (Juggins, 2019). The broken sticks model indicated four main clusters.

3. Results and interpretations

3.1. Sea ice biomarkers

IP_{25} was present in all samples analysed from core AMD14-Kane2b, attesting that Kane Basin was seasonally covered by sea ice during the last *ca* 9 cal. ka BP (Fig. 2). HBI III was detected in all but 6 samples, albeit at much lower concentrations than IP_{25} (i.e. average $[IP_{25}] = 57\ ng{\cdot}g^{-1}$ sediment, average [HBI III] = 1 $ng{\cdot}g^{-1}$ standard equivalent). Both biomarkers however displayed the same general trends in concentrations, with lower values below *ca* 250 cm (*ca* 7.2 cal.

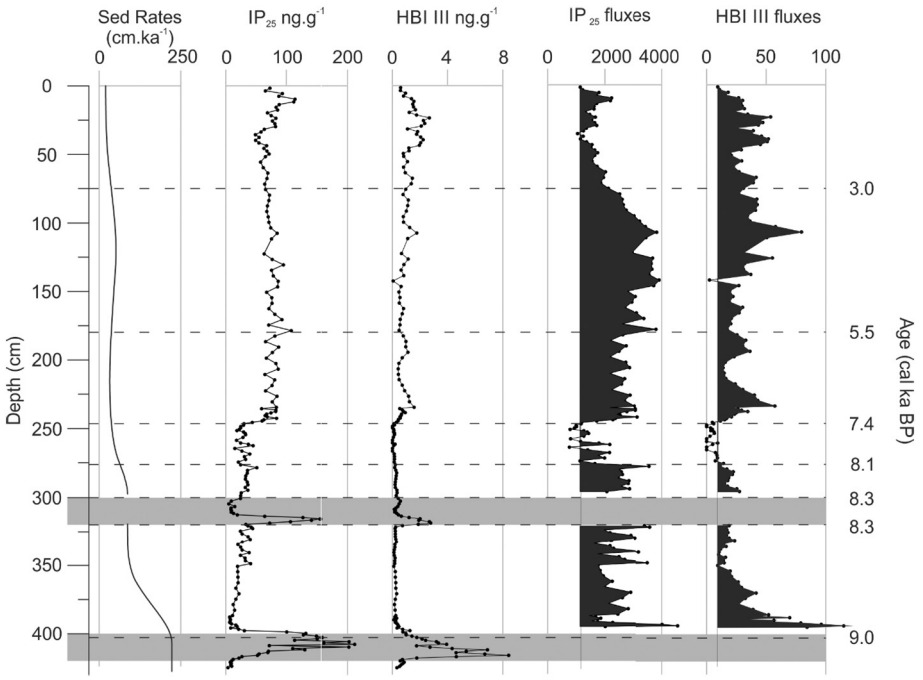

Fig. 2. Sedimentation rates (from Georgiadis et al., 2018), HBI (IP_{25} and HBI III) concentrations and fluxes in core AMD14-Kane2b. The two IRD-rich units are highlighted by grey boxes. Fluxes were not calculated in these two IRD units owing to very high sedimentation rates in these intervals. Fluxes above the value measured at the core top are filled in black, those below appear white. Dashed lines indicate major changes in biomarker fluxes with corresponding ages on the right.

ka BP), higher values above this depth, and very high concentrations in the two IRD-rich intervals. Large sediment inputs at the base of our record, owing to the proximity of glacial ice (Georgiadis et al., 2018), were likely to have caused the lower concentrations in the bottom half of our record. We thus focus on biomarker fluxes rather than concentrations to interpret the record. The variations in biomarker fluxes were compared to the flux measured in the topmost sample of our core which is associated with modern conditions.

The two IRD-rich units at ~400–425 cm and ~300–320 cm, dated at ~9.0 and 8.3 cal. ka BP, were characterised by particularly high concentrations of IP_{25} and HBI III (Fig. 2). Fluxes were not calculated in these two units due to the assumption that they were deposited very rapidly. High amplitude variations of IP_{25} fluxes occurred in the early part of the record from 400 to 320 cm (~9.0 to ~8.3 cal. ka BP). These oscillations may be due to the high temporal resolution owing to higher sedimentation rates (i.e. 1 cm represents an average of only 10 years of sedimentation in this interval) when the IIS and GIS were close to the core site (Georgiadis et al., 2018). Alternatively, or additionally, the proximity of the retreating ice sheets could have provided large amounts of freshwater that may have decreased IP_{25} production, even when seasonal sea ice was effectively present (Ribeiro et al., 2017). The high, but decreasing, HBI III fluxes from *ca* 9.0 to ~8.5 cal. ka BP also point to freshwater input during ice sheet retreat in Kane Basin, in line with the foraminiferal record. The high IP_{25} and HBI III concentrations measured at the base of the IRD-rich unit dated at 8.3 cal. ka BP may have been associated to the breakup of glacial ice in Kennedy Channel (Georgiadis et al., 2018). The mechanical action of calving at an ice margin has been reported to increase productivity (Shadwick et al., 2013) and may have contributed to the high biomarker concentrations. Recurrent seasonal sea-ice between 8.3 and 8.1 cal. ka BP is evidenced by the stable IP_{25} fluxes. This period of sustained high IP_{25} fluxes coincides in time with the 8.2 cal. ka BP cold event and may also have been promoted by the throughflow of cold and fresh Arctic water through Nares Strait. Biomarker fluxes clearly decreased between 8.1 and 7.4 cal. ka BP and were comparable to the low values at the top of our core. IP_{25} fluxes increased sharply at ~250 cm (~7.4 cal. ka BP) and remained high before beginning to decrease at 100 cm (~3.5 cal. ka BP). A smaller increase occurred ~180 cm (*ca* 5.5 cal. ka BP) and IP_{25} fluxes were particularly high between ~150–110 cm (~4.7 and 3.5 cal. ka BP). HBI III fluxes were variable between 250 and 140 cm (~7.4 and 4.5 cal. ka BP), but remained relatively high in the top 140 cm of the core (past ~4.5 cal. ka BP). A minimum in IP_{25} fluxes was reached around 35 cm (~1.7 cal. ka BP), whereas HBI III fluxes were high during this time. This period centred around 1.7 cal. ka BP constitutes the second interval when IP_{25} fluxes were similar to modern values, although HBI III fluxes were higher. A short recovery in IP_{25} fluxes occurred around 10 cm (~0.5 cal. ka BP), while HBI III fluxes decreased. Both IP_{25} and HBI III fluxes decreased in the top 10 cm (over the past 500 years). The decrease in IP_{25} over the past ~3 kyrs, culminating in lower IP_{25} fluxes than present *ca* 1.7 cal. ka BP, can either be interpreted as severe sea ice conditions (i.e. reduced light penetration in very thick sea ice), or as reduced sea ice cover. However, the reasonably high HBI III fluxes during the past 3 kyrs attest to at least occasional occurrence of open water in Kane Basin.

3.2. Foraminifera

Planktic foraminifera were represented exclusively by *Neogloboquadrina pachyderma* sinistral (NPS), a polar species usually the only (dominant) planktic foraminifera present in polar (subpolar) Atlantic water (e.g. Vilks, 1969). NPS concentrations varied between ~0 and 57 ind.g^{-1} dry sediment (Fig. 3). Their fluxes were higher in the earlier part of our record (425–240 cm, *ca* 9.0 to 7.2 cal. ka BP), and decreased until 170 cm (*ca* 5.5 cal. ka BP), after which the occurrence of NPS became rare (Fig. 3).

The concentrations of benthic foraminifera varied between ~0 and 1300 ind.g^{-1} dry sediment (Fig. 3). The base of the core, which is IRD-rich, was barren of foraminifera until 401.5 cm when the abundance of coarse particles decreases (Georgiadis et al., 2018). Fluxes were highest between 280 and 240 cm (~8.1 and 7.2 cal. ka BP), and were also relatively high between 401 and 280 cm (~9.0 and 7.2 cal. ka BP), and between 150 and 60 cm (~4.7 and 2.7 cal. ka BP).

The ecozones defined by the cluster analysis performed on the benthic assemblages were named E1 to E4, and their ages are shown in Fig. 3.

The assemblage composing E1, a single sample dated at ca. 9.0 cal. ka BP (401.5 cm), was largely dominated by *C. reniforme* (~63%), with a subordinate contribution of *Islandiella norcrossi* (~14%). High relative abundances of *C. reniforme* attest to the influence of bottom waters of Atlantic origin at the core site (e.g. Polyak et al., 2002), while *I.*

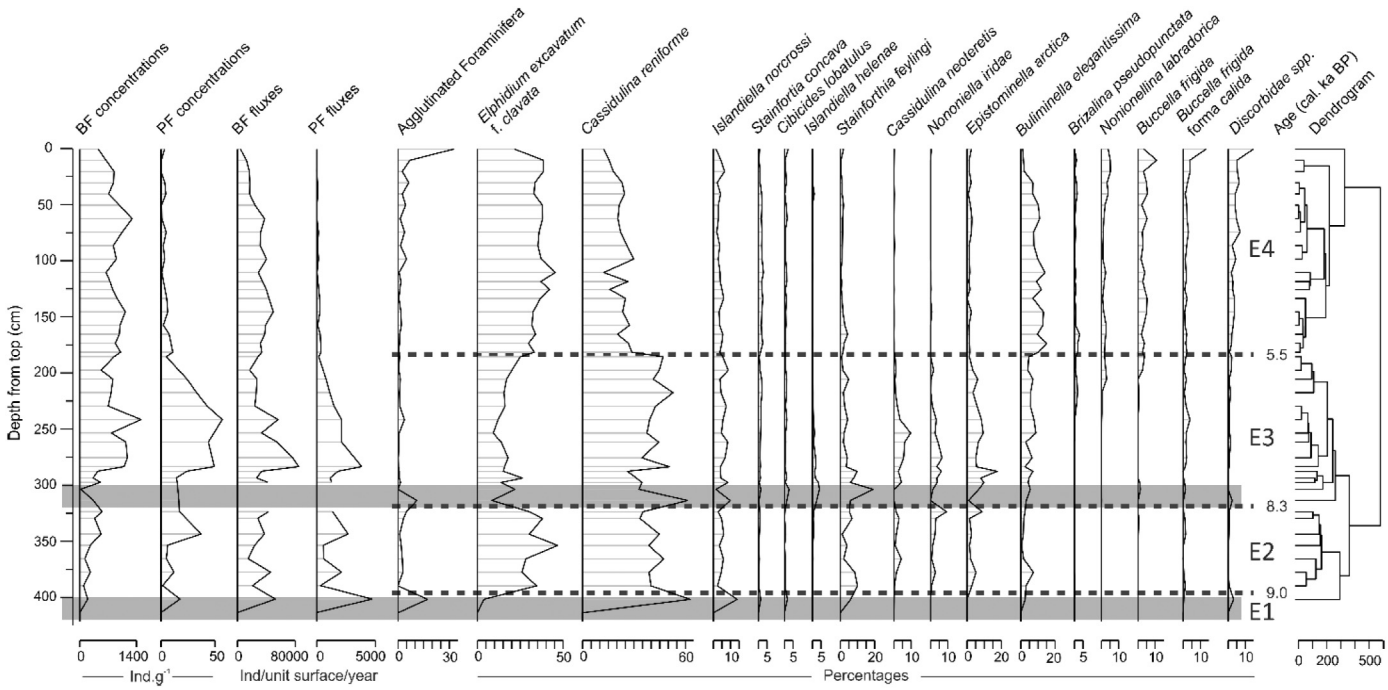

Fig. 3. Benthic (BF) and planktic (PF) foraminifera concentrations and fluxes, percentages of agglutinated foraminifera, abundance of calcareous species in core AMD14-Kane2b, and the hierarchical clustering dendrogram of the distance matrix computed in R. The IRD-rich units are represented by a grey bar along the depth scale. Fluxes were not calculated in the two IRD units owing to very high sedimentation rates in these intervals (Georgiadis et al., 2018).

norcrossi is indicative of stable salinity (Atlantic–sourced) water, possibly under seasonal sea ice (Steinsund and Hald, 1994). We also noted the particularly high abundance of agglutinated foraminifera in this sample (~17% of the total amount of benthic foraminifera) – despite its older age and the method used for sample preparation.

The second assemblage E2 (389.5–323.5 cm, *ca* 8.9–8.3 cal. ka BP) was co-dominated by *E. excavatum* forma *clavata* (~30%) and *C. reniforme* (~40%). Contributions of *I. norcrossi* were reduced in E2 and remain low throughout the rest of the core, while relative abundances of *Stainforthia feylingi* were notable at the base of this interval (up to 10%), and the abundances of *Nononiella iridea* increased up-core (up to 9%). Although low percentages of *Cassidulina neoteritis* were found in E2, their presence was still noteworthy (average of ~2%, with maxima of 4%). The occurrence of the opportunistic species *E. excavatum* forma *clavata* is indicative of unstable environmental conditions and lower salinity (Hald et al., 1994). The presence of *S. feylingi* may also be associated with meltwater inputs in Kane Basin (Jennings et al., 2017). However, chilled Atlantic water was still present in the bottom waters at the core site according to the relatively high abundance of *C. reniforme* (Jennings et al., 2019; Knudsen et al., 2008; Polyak et al., 2002). A limited influence of relatively warmer Atlantic water was also hinted at by the presence of *C. neoteretis* (Jennings et al., 2004), albeit in low numbers. The subordinate contributions of *N. iridea* attest to the pulsed export of phytodetritus to the seabed (e.g. Gooday and Hughes, 2002). This assemblage is representative of a glacimarine environment, with a limited influence of Atlantic water at the bottom and reduced bottom water salinity, possibly due to meltwater inputs, and pulsed productivity related to seasonal sea-ice cover.

The third ecozone E3 (313.5–181.5, *ca* 8.3–5.5 cal. ka BP) was characterised by a sustained dominance of *C. reniforme* (~40%), while contributions of *E. excavatum* forma *clavata* (~17%) were reduced compared to E2. Subordinate species *S. feylingi*, *N. iridea*, *Epistominella arctica*, *Buliminella elegantissima*, and *Cassidulina neoteretis* each contributed to up to 7–19% of the assemblage in E3. The increased contribution of *C. neoteretis* in E3 relative to E2 attests to a greater influence of warmer Atlantic water at the bottom of Kane Basin (Jennings et al., 2004), while the decreasing abundances of *E. excavatum* forma *clavata* and *S. feylingi* point to gradually reduced meltwater. The presence of *N. iridea*, *E. arctica*, and *B. elegantissima* indicate that the export of organic matter occurred in pulses and was related to seasonal sea-ice cover (e.g. Gooday and Hughes, 2002). Ecozone E3 represents a more distal glacial marine environment with reduced meltwater input compared to E2, and maximal Atlantic influence in bottom water at the core site, under seasonal sea-ice cover.

The assemblage of ecozone E4 (181.5–0 cm, ~5.5–0 cal. ka BP) was dominated by *E. excavatum* forma *clavata* (~36%), with lower contribution of *C. reniforme* (~22%). A number of subordinate species in E3 were replaced by *Nonionellina labradorica* (up to 5%) and *Buccella frigida* (up to 11%). The relative abundance of *B. elegantissima*, however, increased to an average of 10% in E4. The notable decrease in *C. reniforme* and *C. neoteretis* abundances compared to the previous ecozone points to a reduced influence of Atlantic bottom water at the core site from *ca* 5.5 cal. ka BP, while increased contributions of *E. excavatum* forma *clavata* is indicative of fresh (possibly polar) water in Kane Basin. The occurrence of the high productivity species *N. labradorica* (Polyak et al., 2002), *B. frigida* (Steinsund and Hald, 1994) and *B. elegantissima* (Knudsen et al., 2008) are indicative of the export of phytodetritus to the seabed, although their individual relative abundances in E4 were on average < 5%. While the decreased influence of Atlantic water in basal water is clear in E4, the precise significance of the replacement of two high productivity species by two others is more complex. It has been suggested that *N. labradorica* may be related to Arctic water masses (Racine, 2019), which supports the interpretation of reduced Atlantic water based on decreased contributions of *C. reniforme* and *C. neoteretis*, and increase fresh polar water based on *E. excavatum* forma *clavata* abundances. In addition, *N. labradorica* has been associated to fresh phytodetritus in polar fronts but not specifically to sea-ice cover (Rytter et al., 2002), whereas *E. arctica* and *N. iridea* are known to withstand long periods of oligotrophic conditions (i.e. severe sea-ice) and to reproduce very rapidly (i.e. more rapidly than other high productivity species) during very brief periods of food supply (e.g. Gooday and Hughes, 2002). Ecozone E4 is thus representative of reduced

Atlantic influence and increased Arctic water in Kane Basin, under seasonal sea-ice cover with significant periods of productivity. This suggests that the decrease in biomarker fluxes in the top part of our record should be interpreted as reduced sea-ice, and not as severe sea-ice cover (cf. 3.1). The overall limited benthic foraminifera fluxes in this likely more productive interval may be due to (1) dissolution of the carbonated taxa, and/or (2) the loss of agglutinated taxa (possibly more competitive in corrosive Arctic waters Aksu, 1983) caused by the sample preparation method.

4. Discussion

The CAA has experienced major environmental changes since the last deglaciation (i.e. past *ca* 18 kyrs) in relation to climatic variability along with eustatic and glacio-isostatic sea-level change (e.g. England et al., 2006). The present study provides the first long-term proxy record of sea-ice cover and oceanographic changes in Kane Basin. Both our micropaleontological and biogeochemical datasets suggest that Kane Basin was seasonally covered by sea ice during the last 9.0 kyrs. However, changes in biomarker fluxes and benthic foraminiferal assemblages suggest variability in sea-ice dynamics and ocean circulation. Here, we discuss the history of paleoenvironmental conditions in Kane Basin in response to changing local geomorphology and regional climate during and following the deglaciation of Nares Strait.

4.1. Deglaciation of Kane Basin (ca 9.0–8.3 cal. ka BP)

In line with sedimentological evidence previously shown by Georgiadis et al. (2018), a transition from an ice sheet-marginal to ice-distal environment was recorded by our micropaleontological and biomarker data from *ca* 9.0 to 8.3 cal. ka BP. The co-dominance of *C. reniforme* and *E. excavatum* forma *clavata* attest to a glacimarine environment under the influence of Atlantic water in Kane Basin during this interval (Fig. 4). The sediment at the base of our core displayed relatively high concentrations of sea-ice biomarkers and were likely deposited close to the ice margin. Ice marginal environments can be productive owing to the upwelling of nutrients through meltwater plumes, the stratification induced by meltwater inputs (e.g. Kanna et al., 2018), and the mechanically induced breakup of sea ice by calving (Shadwick et al., 2013). Both highly variable IP_{25} fluxes and high percentages of *E. excavatum* forma *clavata* suggest unstable salinity and likely variable sea-ice cover in Kane Basin between *ca* 9.0 and 8.3 cal. ka BP (Fig. 4). These unstable conditions are possibly the result of freshwater input and a local cooling owing to the proximity of the GIS and IIS, and high atmospheric temperatures during the Holocene Thermal Maximum (HTM, Fig. 5; Lecavalier et al., 2017). In Smith Sound, to the south of Nares Strait, benthic foraminiferal assemblages are indicative of a transition from harsh environmental conditions with a strongly stratified water column and severe sea-ice cover, towards more seasonal sea-ice and productive surface waters starting around 9 cal. ka BP (Jennings et al., 2019). This temporal disparity between the two core sites reflects the northward retreat of the IIS and the GIS in southern Nares Strait.

The IRD-rich unit dated at ~8.3 cal. ka BP in core AMD14-Kane2b has been interpreted to mark the opening of the Kennedy Channel (Georgiadis et al., 2018) and is characterised by high concentrations of sea ice biomarkers. High calving rates associated with the deglaciation of Kennedy Channel may have fuelled sea ice and ice margin productivity in Kane Basin by mechanically enhancing light availability due to sea ice break-up. Alternatively, this IRD-rich unit may have been deposited by the retreat of the Humboldt Glacier happening around this time (Reusche et al., 2018).

4.2. Maximum influence of Atlantic Water in Kane Basin (ca 8.3–7.4 cal. ka BP)

The period between 8.3 and 7.4 cal. ka BP is marked by a maximum in Atlantic influence in the bottom water of Kane Basin as suggested by the dominance of *C. reniforme* and the presence of *C. neoteritis*. Biomarker fluxes are variable, indicating changes in sea ice cover during this interval. The ingress of Atlantic water into Kane Basin may have been facilitated by the greater water depth prior to the postglacial isostatic rebound (up to 120–140 m deeper; England et al., 2006). The modern Nares Strait bottom water characteristic implies that Arctic-sourced Atlantic Water lying at 350 m water depth must surpass a sill (300 m water depth) to enter Nares Strait from the north (Münchow et al., 2011), or face the upward sloping Kane Basin topography for Baffin Bay-sourced Atlantic water entering via the south (e.g. Münchow, 2016). Up to 120–140 m greater water depth in Nares Strait prior to the rebound would have facilitated the entrance of Atlantic water at depth, both through the north and the south. A short period (*ca* 8.3–8.1 cal. ka BP) of high IP_{25} and relatively low HBI III fluxes follows the IRD-rich unit and coincides with the 8.2 event recorded in the nearby Agassiz ice core record (Figs. 4 and 5; Lecavalier et al., 2017). This cold event is thought to have been triggered by the drainage of the proglacial Agassiz lakes (Barber et al., 1999). Locally, the cooling may have been accentuated by increased fluxes of freshwater and cold air through Nares Strait associated with the newly-established connection of the Arctic Ocean to Baffin Bay. The increased freshwater flux through the strait may have promoted recurrent (and possibly occasionally perennial) sea-ice cover in Kane Basin during this cold period. Heavy sea-ice cover is supported by the occurrence of *S. feylingi* and *E. arctica* (Fig. 4). The link between the 8.2 event and extensive sea-ice cover in Kane Basin may however be coincidental, since the error associated to our age model is approximately ± 200 years owing to reservoir age corrections alone (Georgiadis et al., 2018). Biomarker fluxes reach minimal values (some below those measured at the core top) between *ca* 8.1 and 7.4 cal. ka BP, coinciding with persisting high atmospheric temperatures of the HTM in the region (Fig. 5; Lecavalier et al., 2017). Low IP_{25} fluxes suggest that sea-ice cover in Kane Basin was reduced during this time, possibly with a shorter sea-ice season on a yearly basis. The maximum influence of (warmer) Atlantic water in Kane Basin at this time may have promoted more open water at the surface, along with more glaciodistal conditions as the GIS and IIS retreated. Alternatively, the throughflow of Arctic surface water through Nares Strait and increased meltwater input into Kane Basin during this warmer period could have been detrimental to IP_{25}-producing diatoms (Ribeiro et al., 2017). Dinocyst assemblages from core AMD14-Kane2b, which are largely dominated by heterotrophic taxa, display a short-lived increase of autotrophic species during this interval, supporting slightly warmer, more open-water conditions in Kane Basin (Caron et al., 2019). Nil to minimum HBI III fluxes suggest a reduced influence of marginal ice conditions at the core site between *ca* 8.1 and 7.4 cal. ka BP. Both the decrease in HBI III and IP_{25} fluxes may have been caused by earlier spring melt of sea ice. An increase in seasonal open water conditions is also supported by the peak in both planktic and benthic foraminifera fluxes. In addition, it is worth noting that the occurrence of landfast sea ice in the Lincoln Sea was scarce during the Early Holocene, according to driftwood records from northern Ellesmere Island (Fig. 5; England et al., 2008). Our record of foraminifera and sea-ice biomarker fluxes supports the fact that sea-ice occurrence in the Nares Strait area was relatively low between *ca* 8.1 and 7.4 cal. ka BP, following a period of potentially sustained sea ice cover between 8.3 and 8.1 cal. ka BP (Fig. 4).

4.3. Increased drift-ice and shallowing of Kane Basin (ca 7.4–5.5 cal. ka BP)

The benthic foraminiferal assemblage in ecozone E3 and high

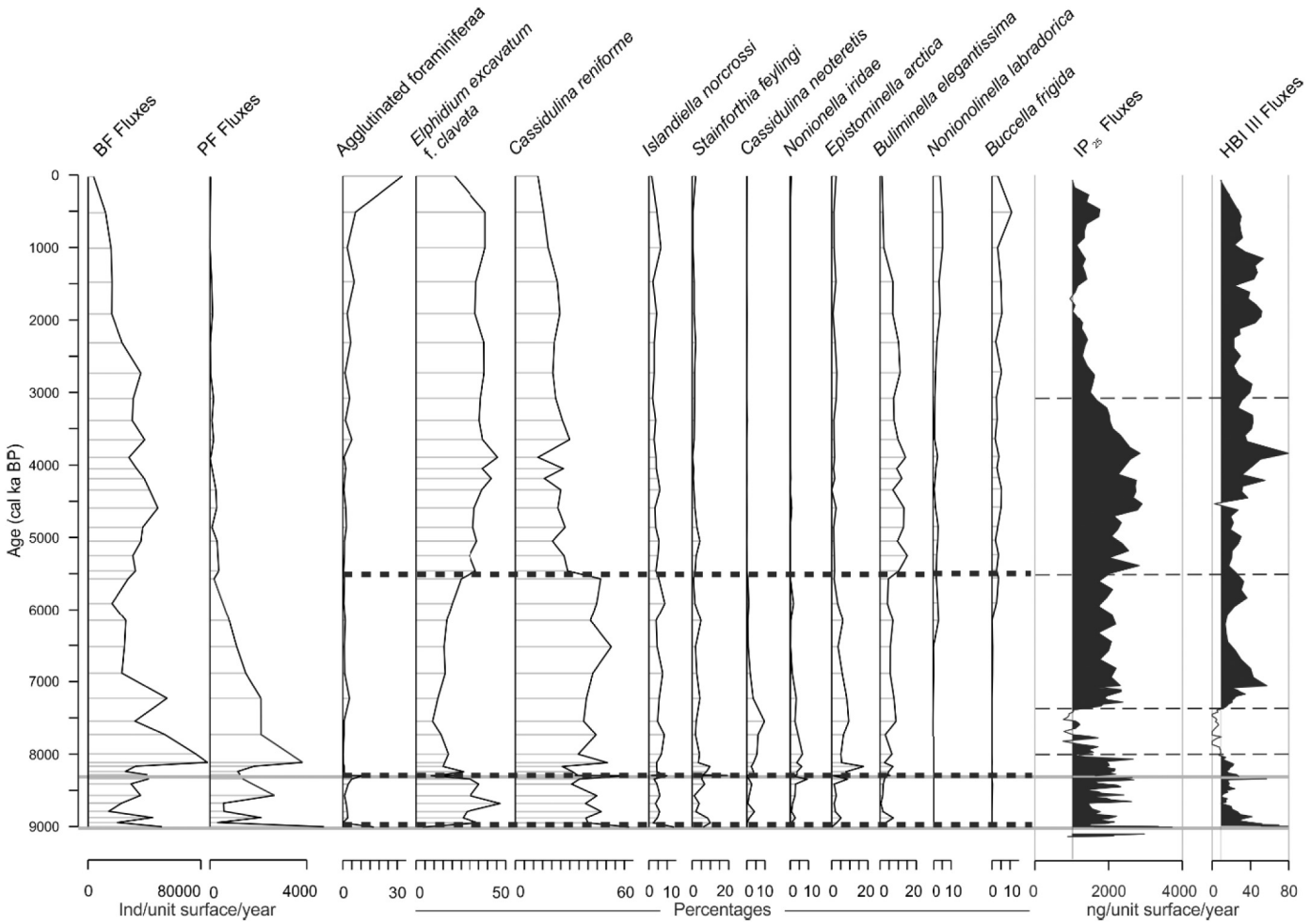

Fig. 4. Benthic (BF) and planktic (PF) foraminifera fluxes, percentage of agglutinated foraminifera, and abundance of the benthic foraminifera species used to reconstruct paleoenvironment in Kane Basin, plotted next to IP_{25} and HBI III fluxes in core AMD14-Kane2b on an age scale. Thick dashed lines delimitate ecozones and thin dashed lines indicate changes in biomarker fluxes. The two IRD-rich units are represented by grey solid lines.

planktic foraminifera fluxes are indicative of a strong influence of Atlantic water in Kane Basin between *ca* 8.3 and 5.5 cal. ka BP and a gradual reduction of Atlantic water starting *ca* 7.4 with decreasing numbers of *C. neoteretis* and planktic foraminifera (Fig. 4). The post-glacial isostatic rebound likely began with the thinning of the GIS and IIS during the Early Holocene (Lecavalier et al., 2014), but the effects of the shallowing of Kane Basin are most apparent in our record between *ca* 7.4 and 5.5 cal. ka BP. The decrease in warm Atlantic indicator species suggests a progressively reduced presence of Atlantic water associated with the shoaling of Nares Strait. Their replacement by *E. excavatum* forma *clavata* from *ca* 5.5 cal. ka BP is indicative of fresher bottom water in Kane Basin, similar to the modern oceanographic circulation which is characterised by limited Atlantic water and predominantly Arctic water masses.

A pronounced increase in biomarker fluxes occurred *ca* 7.4 cal. ka BP. The sustained high IP_{25} fluxes indicate an increase in sea-ice cover in Kane Basin between *ca* 7.4 and 5.5 cal. ka BP. This coincides with a decrease in atmospheric temperatures *ca* 7.5 cal. ka BP following the end of the HTM (Fig. 5; Lecavalier et al., 2017). Interestingly, this also corresponds to a period of maximum driftwood deposition in northern Ellesmere Island (*ca* 7.0–5.5 cal. ka BP; Fig. 5; England et al., 2008), likely caused by enhanced sea ice in the Arctic Ocean as atmospheric temperatures dropped (Fig. 5; Lecavalier et al., 2017). A marked decrease in July air temperatures is also inferred by chironomid assemblages recovered in sediments from a nearby lake (Axford et al., 2019). Although sea-ice cover may have been present in Kane Basin during this time, we refrain from affirming that the ice arches existed in Nares Strait between 7.5 and 5.5 cal. ka BP. This is based on the fact that there is no evidence to date of (1) the opening of a polynya in northernmost Baffin Bay during this interval (Davidson et al., 2018) nor (2) landfast ice in northern Ellesmere Island that could have formed a recurrent northern ice arch (England et al., 2008). The relatively low abundances of sea-ice diatoms in the North Water (NOW) area between *ca* 7.3 and 5.5 cal. ka BP (Knudsen et al., 2008) does not suggest that northernmost Baffin Bay was so severely ice-covered that the opening of the polynya may have been prevented by in situ sea-ice formation were the Kane Basin ice arch indeed present. Instead, we propose that, although Arctic sea-ice cover increased with lower atmospheric temperatures, winter atmospheric temperatures were not yet low enough to allow the formation of sufficiently thick ice in the Lincoln Sea and in Kane Basin to withstand the strong, along strait winds. Furthermore, according to the origin and the spatial distribution of driftwood between northern Ellesmere Island and Northern Greenland, positive phases of the Arctic Oscillation (AO) prevailed from *ca* 8.5 and 6.0 cal. ka BP (Fig. 5; Funder et al., 2011). During modern AO positive phases, the atmospheric Beaufort High likely extends over the Lincoln Sea (Steele et al., 2004), perhaps explaining the correlation between wind strength in Nares Strait and the AO index in modern times (Samelson and Barbour, 2008; Fig. 6). The strong winds during this period of prevailing positive phases of the AO may have been unfavourable to ice arch formation (Dumont et al., 2009). The overall increase in HBI III fluxes between *ca* 7.4–5.5 cal. ka BP suggests ice-loaded fresh surface water in Kane Basin.

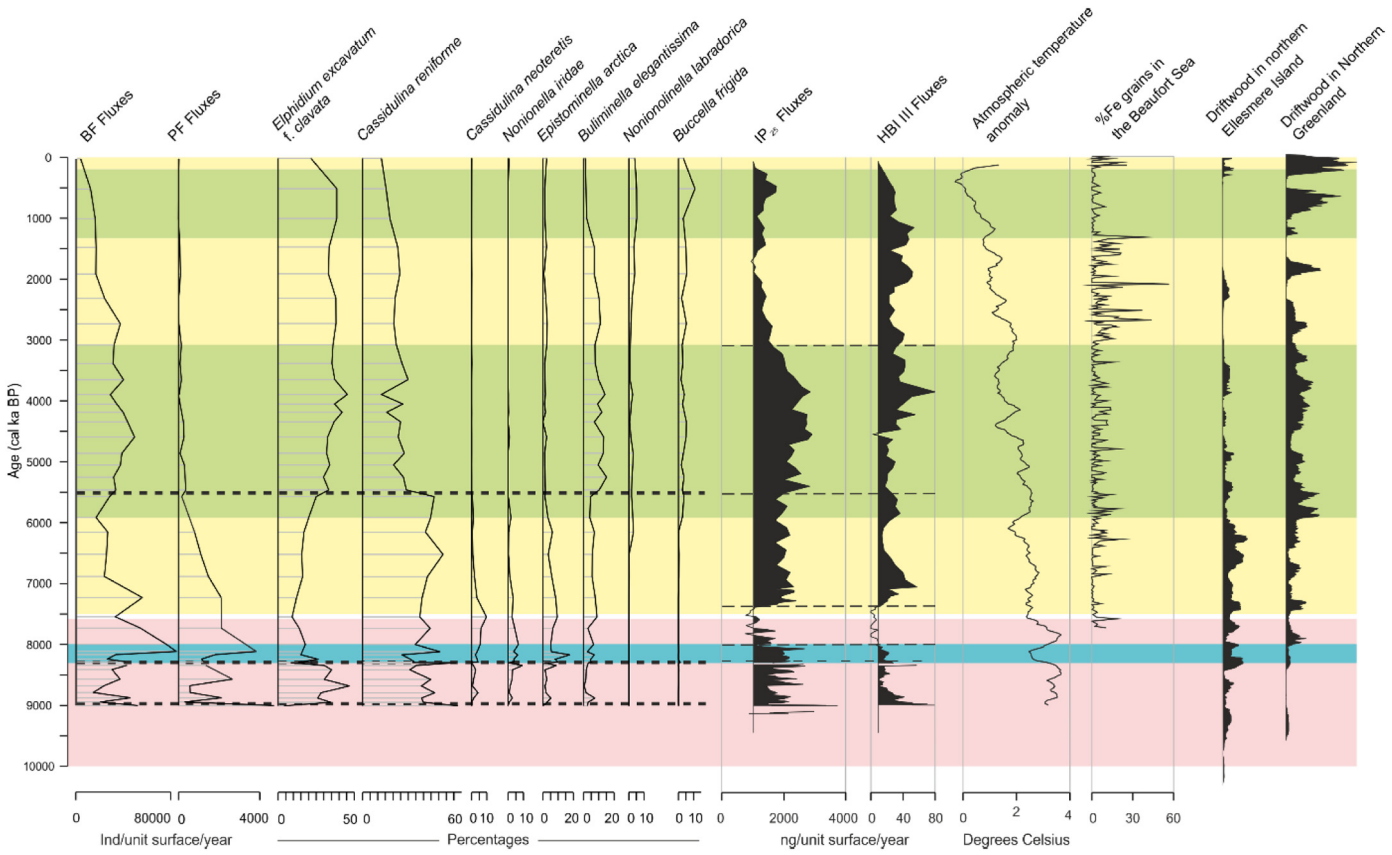

Fig. 5. Comparison of benthic (BF) and planktic (PF) foraminifera fluxes, abundance of selected benthic foraminifera species, and IP_{25} and HBI III fluxes in AMD14-Kane2b with regional records, including the temperature anomaly (°C, from $\delta^{18}O$) (Lecavalier et al., 2017), Siberian IRD in the Beaufort Gyre (Darby et al., 2012), cumulative probability distribution of calibrated ^{14}C ages of driftwood in northern Ellesmere Island (England et al., 2008) and north-eastern Greenland (Funder et al., 2011). The HTM is marked in red, and the 8.2 cold event in blue (based on the Agassiz temperature record). AO positive phases are represented in yellow, AO negative in green. (For interpretation of the references to colour in this figure legend, the reader is referred to the web version of this article.)

These surface conditions are consistent with high mobile sea-ice and freshwater flux through Nares Strait in the absence of ice arches and under the influence of strong northerly winds.

4.4. Establishment of modern oceanography in Nares Strait and the inception of ice arches (ca 5.5–3.0 cal. ka BP)

A further increase in IP_{25} fluxes occurs *ca* 5.5 cal. ka BP and coincides with a change in benthic foraminiferal assemblage (Fig. 4). *E. excavatum* forma *clavata* replaces *C. reniforme* as the dominant species, attesting to a major shift in bottom water masses as they are represented by fresher water while the influence of Atlantic water is reduced following the shoaling of Kane Basin. The notable contributions of phytodetritus index species *N. labradorica*, *B. frigida*, and *B. elegantissima*, in the foraminiferal assemblage over the past 5.5 kyrs suggests the seasonal export of fresh organic matter related to ice-edge productivity in Kane Basin. Later sea-ice retreat, in phase with the insolation maximum in the late spring or early summer, may have enhanced the export of organic matter since under-ice and ice-edge environments are more productive than open water (Mayot et al., 2018). Higher IP_{25} fluxes are also suggestive of a longer sea-ice productivity season (Belt and Müller, 2013). We propose that this later retreat of the sea ice in Kane Basin is likely linked to the onset of the recurrent, seasonal formation of a stable ice arch in Kane Basin. According to Funder et al. (2011), negative phases of the AO prevailed from *ca* 6 cal. ka BP. Along with the Neoglacial cooling, negative phase of the AO could have promoted the formation of ice arches in Nares Strait through two main processes (Fig. 6). Firstly, sea ice thickness in the Arctic Ocean is negatively correlated to the AO index due to the atmospheric control on sea-ice circulation (Rigor et al., 2002). Secondly, weaker winds in Nares Strait during negative phases of the AO (Samelson and Barbour, 2008) are less likely to break-up landfast ice (Dumont et al., 2009). Together, colder atmospheric temperatures, thicker sea ice, and weaker winds between *ca* 5.5 and 3.0 cal. ka BP could have promoted ice arch formation in Nares Strait.

The changes observed in our Kane Basin proxy records at *ca* 5.5 cal. ka BP are near synchronous with the development of ice shelves (Antoniades et al., 2011) and thick coastal ice (England et al., 2008) in northern Ellesmere Island. The development of these ice shelves may be linked to the establishment of the seasonal northern ice arch in Nares Strait. Benthic foraminiferal assemblages from the NOW display reduced abundances of *E. excavatum* forma *clavata* and increased contributions of *N. labradorica ca* 5.2 cal. ka BP, suggesting a transition from harsh conditions towards a productive polar front with seasonal sea ice (Knudsen et al., 2008). This more productive environment could be linked to occasional openings of a polynya due to an infrequent ice arch in Kane Basin. However, according to Davidson et al. (2018) the inception of the NOW polynya did not occur before *ca* 4.5 cal. ka BP (Davidson et al., 2018), which raises the question of whether the southern ice arch was firmly established between 5.5 and 4.5 cal. ka BP (Fig. 5). Our biomarker records display a slight increase in IP_{25} fluxes *ca* 4.7 cal. ka BP, which may correspond to a more recurrent southern ice arch around the time of the inception of the NOW polynya.

4.5. Decline of sea ice cover in Kane Basin (ca 3.0–0 cal. ka BP)

IP_{25} fluxes in Kane Basin decrease after *ca* 3.0 cal. ka BP indicating a decline in sea ice cover despite continued atmospheric cooling (Fig. 5;

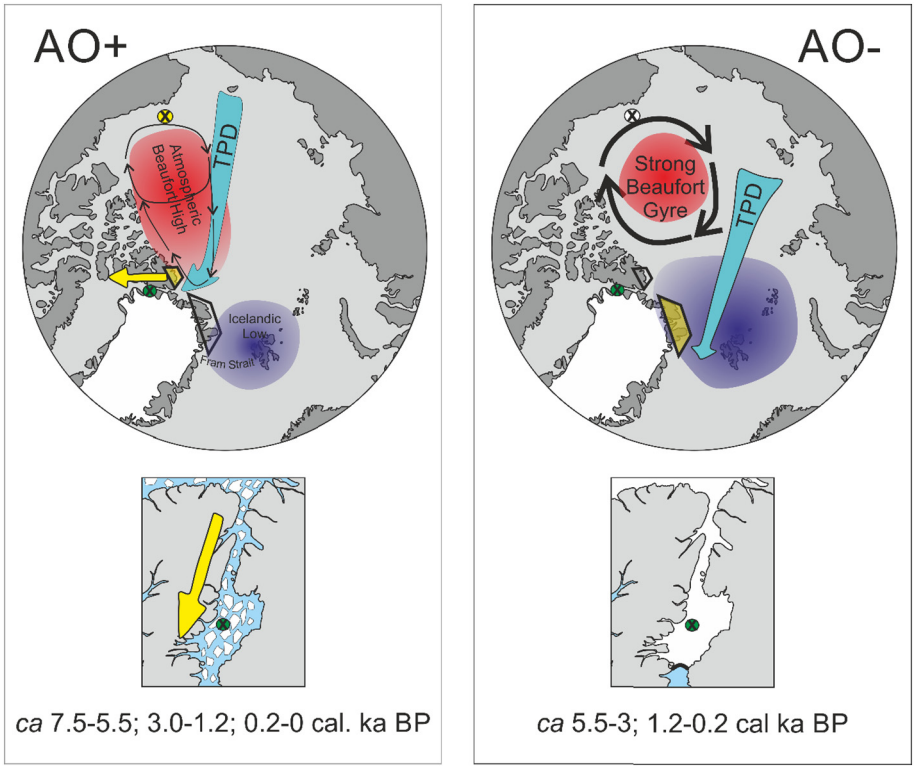

Fig. 6. Schematic representation of positive (+) and negative (−) phases of the Arctic Oscillation (AO), and of sea ice conditions in Nares Strait, adapted from Steele et al. (2004). Location of core AMD14-Kane2b is marked by a cross in a green circle (this study), the record of IRD in the Beaufort Sea is marked by a cross in a yellow (AO+) or white (AO−) circle (Darby et al., 2012). The study area of driftwood occurrence in northern Ellesmere Island (England et al., 2008), and in Northern Greenland (Funder et al., 2011) are marked by trapezoids. In a positive phase of the AO, the Beaufort Gyre is weak (unfavourable to multi-year sea ice), the atmospheric Beaufort High (red) extends into the Lincoln Sea, and the transpolar drift (TPD, carrying Siberian IRD to the Beaufort Sea and driftwood to northern Ellesmere Island) originates in eastern Siberia and funnels ice towards Nares Strait. The pressure difference between northern and southern Nares Strait is strong during positive AO phases, leading to strong, along-strait winds (yellow arrow). Both thinner Arctic sea ice and strong winds are unfavourable to ice arch formation in Nares Strait under positive AO conditions. During a negative phase of the AO, a strong Beaufort gyre promotes multi-year sea ice, while the TPD takes a more direct route towards Fram Strait, and deposits driftwood in Northern Greenland. The extension of the Icelandic Low (blue) into the Arctic Ocean potentially creates low pressure in the Lincoln Sea, reducing the pressure gradient along Nares Strait. Thick multi-year sea ice and weaker winds promote the formation of ice arches in Nares Strait under negative AO phases. (For interpretation of the references to colour in this figure legend, the reader is referred to the web version of this article.)

Lecavalier et al., 2017). Darby et al. (2012) report strong positive phases of the AO starting *ca* 3.0 cal. ka BP based on an IRD record in the Beaufort Sea (Fig. 5). Prevailing positive AO phases are also supported by a decrease in driftwood occurrence in Northern Greenland (Funder et al., 2011). Stronger winds may have favoured the export of sea ice through Nares Strait and hindered the formation of the Kane Basin ice arch during this period, explaining the low IP_{25} fluxes (Fig. 6). The decay of Little Auk colonies in Thule after *ca* 3.0 cal. ka BP is probably a result of an unstable southern ice arch in Kane Basin under these conditions. Lowest IP_{25} fluxes occurred between *ca* 2.2 and 1.1 cal. ka BP (Fig. 5). IP_{25} fluxes recover briefly around 0.5 cal. ka BP, as more negative phases of the AO are inferred by driftwood in Northern Greenland (Funder et al., 2011) and the IRD record in the Beaufort Sea (Darby et al., 2012). A decrease in IP_{25} fluxes towards the core top coincides with increasing positive phases of the AO over the past two centuries (Darby et al., 2012), and warmer atmospheric temperatures (Lecavalier et al., 2017). We note that while the southern ice arch in Kane Basin appears to have been weaker over the past *ca* 3 kyrs than it was between 4.5 and 3.0 cal. ka BP, the northern ice arch was likely a recurrent feature in the Lincoln Sea during this time according to the paucity of driftwood in northern Ellesmere Island (England et al., 2008). The fact that the northern ice arch was present during this interval may explain the little change in our foraminiferal assemblages. The assemblage is similar to the previous interval, indicating a productive ice edge environment. The presence of the northern ice arch after 5.5 cal. ka BP likely limited the export of Arctic drift-ice through Nares Strait and promoted high productivity rates, as opposed to the interval between 7.4 and 5.5 cal. ka, when the northern ice arch was absent and productivity was hindered by the passing of drift-ice through Nares Strait. However, recent instabilities have also been recognised in the northern ice arch during the 20th century (England et al., 2008), and more recently since the early 2000s (Kwok et al., 2010; Moore and McNeil, 2018). This suggests that we may currently be witnessing a shift of surface conditions in Kane Basin towards those reported between 7.4 and 5.5 cal. ka BP (i.e. absence of both ice arches, increased sea ice export through Nares Strait, and decreased productivity under prevailing AO positive phases and warm atmospheric temperatures), or even towards HTM surface conditions reported between 8.1 and 7.5 cal. ka BP (i.e. very low sea ice cover, absence of ice arches, and limited productivity).

5. Conclusion

Our biomarker and foraminiferal datasets provide the first records of Holocene environmental conditions in Kane Basin related to ocean circulation and sea-ice dynamics. Our results indicate that the establishment or the collapse of recurrent ice arches in Nares Strait throughout the last 9000 years are synchronous with major shifts in Arctic sea ice and atmospheric circulation patterns related to the Arctic Oscillation, while changes in ocean circulation in Kane Basin are likely linked to the postglacial rebound. Our reconstructions of surface conditions in Kane Basin and our hypothesis concerning the local and regional factors controlling sea-ice dynamics and oceanographic circulation in Nares Strait can be summarised as follows:

- A glacimarine environment with highly variable sea-ice cover persisted during ice sheet retreat in Kane Basin between *ca* 9.0 and 8.3 cal. ka BP, and was influenced by warm atmospheric temperatures during the HTM and possibly by the local cooling effect of the IIS and GIS.
- Maximal influence of Atlantic water characterised the interval between *ca* 8.3 and 7.5 cal. ka BP, when Kane Basin was deeper prior to the isostatic rebound. Minimal sea ice cover is inferred by low biomarker fluxes between 8.1 and 7.4 cal. ka BP, during the end of

the HTM and in a more glacio-distal environment.

- Mobile Arctic drift-ice likely passed through Nares Strait in the absence of the northern and southern ice arches during prevailing positive phases of the AO between *ca* 7.5 and 5.5 cal. ka BP, hindering productivity, while Atlantic water was progressively excluded from Kane Basin by the postglacial uplift.
- Together with cooler atmospheric temperatures, a shift towards more negative phases of the AO may have favoured increased duration of sea ice occurrence and the establishment of ice arches in Nares Strait between *ca* 5.5 (northern ice arch) or *ca* 4.5 (southern ice arch) and 3.0 cal. ka BP.
- Prevailing positive phases of the AO starting *ca* 3.0 cal. ka BP coincide with the beginning of recent instabilities in the Kane Basin ice arch, while a brief recovery of this southern ice arch occurred during more negative phases of the AO between *ca* 1.2 and 0.2 cal. ka BP. Productivity in Kane Basin likely remained high owing to the presence of the northern ice arch during this time.

While we have focussed on shifts in the Arctic Oscillation to explain the changes in surface conditions in Kane Basin, it must be acknowledged that other secondary modes of sea level pressure variations (e.g. Barent Oscillation (Smedsrud et al., 2013), Dipole Anomaly (Wang et al., 2009)), along with thermodynamic factors (Kwok and Untersteiner, 2011), play significant roles in oceanic and atmospheric circulation in the Arctic Ocean and, in particular, sea ice export towards lower latitudes. However, the availability of records of the AO covering the Holocene, along with the potentially dominant role of the AO on longer time scales (e.g. build-up of sea ice in the Arctic Ocean which preconditions its response to secondary modes (Dumas et al., 2003)), justified the focus of our work on this index. The apparent link between the AO index and ice arch formation in Nares Strait implies that the recently observed instabilities of the ice arches are prone to continue with the predicted positive phases of the AO in the near-future (Rigor et al., 2002). These instabilities are likely to severely impact the NOW polynya area (Marchese et al., 2017), and may influence convection patterns as far as the Labrador Sea (Belkin et al., 1998) as sea-ice and freshwater export through Nares Strait increase in the absence of ice arches (Münchow, 2016).

Declaration of competing interest

The corresponding author (Eleanor Georgiadis) states that there is no conflict of interest.

Acknowledgements

Eleanor Georgiadis' studentship is funded by the Iniative d'Excellece (IdEx) programme of the University of Bordeaux, and the Natural Science and Engineering Research Council of Canada (NSERC). We warmly thank Benoit Lecavalier for constructive conversations, and for having shared with us the Agassiz ice core temperature record and simulations of sea level change in Nares Strait. Our gratitude is also extended to Naima El Bani Altuna, Frédérique Eynaud and Jérôme Bonnin for discussions concerning foraminifera, and Caroline Guilmette for analytical support for HBI measurements. We thank the editor, Adina Paytan, for entrusting our original manuscript to both a paleoceanographer and a physical oceanographer in the reviewing process. The manuscript was greatly improved thanks to both reviewers' comments. This work is supported by the Fondation Total, the French Agence Nationale de la Recherche (GreenEdge project), the Network of Centres of Excellence ArcticNet, and the European Research Council (StG IceProxy). Finally, we wish to thank the CCGS *Amundsen* captain, officers and crew for their support during the 2014 ArcticNet cruise.

Data availability

All data is available on request (eleanor.georgiadis@u-bordeaux.fr).

References

Aksu, A.E., 1983. Holocene and Pleistocene dissolution cycles in deep-sea cores of Baffin Bay and Davis Strait: palaeoceano-graphic implications. Mar. Geol. 53, 331–348. https://doi.org/10.1016/0025-3227(83)90049-X.

Antoniades, D., Francus, P., Pienitz, R., St-Onge, G., Vincent, W.F., 2011. Holocene dynamics of the Arctic's largest ice shelf. Proc. Natl. Acad. Sci. 201106378. https://doi.org/10.1073/pnas.1106378108.

Axford, Y., Lasher, G.E., Kelly, M.A., Osterberg, E.C., Landis, J., Schellinger, G.C., Pfeiffer, A., Thompson, E., Francis, D.R., 2019. Holocene temperature history of northwest Greenland – with new ice cap constraints and chironomid assemblages from Deltasø. Quat. Sci. Rev. 215, 160–172. https://doi.org/10.1016/j.quascirev.2019.05.011.

Barber, D.C., Dyke, A., Hillaire-Marcel, C., Jennings, A.E., Andrews, J.T., Kerwin, M.W., Bilodeau, G., McNeely, R., Southon, J., Morehead, M.D., Gagnon, J.-M., 1999. Forcing of the cold event of 8,200 years ago by catastrophic drainage of Laurentide lakes. Nature 400, 344. https://doi.org/10.1038/22504.

Barber, D.G., Hanesiak, J.M., Chan, W., Piwowar, J., 2001. Sea-ice and meteorological conditions in Northern Baffin Bay and the North Water polynya between 1979 and 1996. Atmosphere-Ocean 39, 343–359. https://doi.org/10.1080/07055900.2001.9649685.

Belkin, I.M., Levitus, S., Antonov, J., Malmberg, S.-A., 1998. "Great Salinity Anomalies" in the North Atlantic. Prog. Oceanogr. 41, 1–68.

Belt, S.T., Müller, J., 2013. The Arctic sea ice biomarker IP25: a review of current understanding, recommendations for future research and applications in palaeo sea ice reconstructions. Quat. Sci. Rev. 79, 9–25. https://doi.org/10.1016/j.quascirev.2012.12.001.

Belt, S.T., Vare, L.L., Massé, G., Manners, H.R., Price, J.C., MacLachlan, S.E., Andrews, J.T., Schmidt, S., 2010. Striking similarities in temporal changes to spring sea ice occurrence across the central Canadian Arctic Archipelago over the last 7000 years. Quat. Sci. Rev. 29, 3489–3504. https://doi.org/10.1016/j.quascirev.2010.06.041.

Brown, T.A., Belt, S.T., Tatarek, A., Mundy, C.J., 2014. Source identification of the Arctic sea ice proxy IP_{25}. Nat. Commun. 5, 4197. https://doi.org/10.1038/ncomms5197.

Caron, M., Rochon, A., Montero-Serrano, J., St-Onge, G., 2019. Evolution of sea-surface conditions on the northwestern Greenland margin during the Holocene. J. Quat. Sci. 34 (7), 569–580. https://doi.org/10.1002/jqs.3146.

Caron, M., St-Onge, G., Montero-Serrano, J.-C., Rochon, A., Georgiadis, E., Giraudeau, J., Massé, G., 2019. Holocene chronostratigraphy of northeastern Baffin Bay based on radiocarbon and palaeomagnetic data. Boreas 48, 147–165. https://doi.org/10.1111/bor.12346.

Darby, D.A., Ortiz, J.D., Grosch, C.E., Lund, S.P., 2012. 1,500-year cycle in the Arctic Oscillation identified in Holocene Arctic sea-ice drift. Nat. Geosci. 5, 897–900. https://doi.org/10.1038/ngeo1629.

Davidson, T.A., Wetterich, S., Johansen, K.L., Grønnow, B., Windirsch, T., Jeppesen, E., Syväranta, J., Olsen, J., González-Bergonzoni, I., Strunk, A., Larsen, N.K., Meyer, H., Søndergaard, J., Dietz, R., Eulears, I., Mosbech, A., 2018. The history of seabird colonies and the North Water ecosystem: Contributions from palaeoecological and archaeological evidence. Ambio 47, 175–192. https://doi.org/10.1007/s13280-018-1031-1.

Dumas, J.A., Flato, G.M., Weaver, A.J., 2003. The impact of varying atmospheric forcing on the thickness of arctic multi-year sea ice. Geophys. Res. Lett. 30. https://doi.org/10.1029/2003GL017433.

Dumont, D., Gratton, Y., Arbetter, T.E., 2009. Modeling the dynamics of the North Water polynya ice bridge. J. Phys. Oceanogr. 39, 1448–1461. https://doi.org/10.1175/2008JPO3965.1.

Dunbar, M., 1969. The geographical position of the North Water. Arctic 22, 438–441.

England, J., 1999. Coalescent Greenland and Innuitian ice during the last glacial maximum: revising the Quaternary of the Canadian High Arctic. Quat. Sci. Rev. 18, 421–456. https://doi.org/10.1016/S0277-3791(98)00070-5.

England, J., Atkinson, N., Bednarski, J., Dyke, A.S., Hodgson, D.A., Ó Cofaigh, C., 2006. The Innuitian Ice Sheet: configuration, dynamics and chronology. Quat. Sci. Rev. 25, 689–703. https://doi.org/10.1016/j.quascirev.2005.08.007.

England, J.H., Lakeman, T.R., Lemmen, D.S., Bednarski, J.M., Stewart, T.G., Evans, D.J.A., 2008. A millennial-scale record of Arctic Ocean sea ice variability and the demise of the Ellesmere Island ice shelves. Geophys. Res. Lett. 35. https://doi.org/10.1029/2008GL034470.

Funder, S., Goosse, H., Jepsen, H., Kaas, E., Kjær, K.H., Korsgaard, N.J., Larsen, N.K., Linderson, H., Lyså, A., Möller, P., Olsen, J., Willerslev, E., 2011. A 10,000-year record of Arctic Ocean sea-ice variability—view from the beach. Science 333, 747–750. https://doi.org/10.1126/science.1202760.

Georgiadis, E., Giraudeau, J., Martinez, P., Lajeunesse, P., St-Onge, G., Schmidt, S., Massé, G., 2018. Deglacial to postglacial history of Nares Strait, Northwest Greenland: a marine perspective from Kane Basin. Clim. Past 14, 1991–2010. https://doi.org/10.5194/cp-14-1991-2018.

Gooday, A.J., Hughes, J.A., 2002. Foraminifera associated with phytodetritus deposits at a bathyal site in the northern Rockall Trough (NE Atlantic): seasonal contrasts and a comparison of stained and dead assemblages. Mar. Micropaleontol. 46, 83–110. https://doi.org/10.1016/S0377-8398(02)00050-6.

Grimm, E.C., 1987. CONISS: a FORTRAN 77 program for stratigraphically constrained cluster analysis by the method of incremental sum of squares. ScienceDirect [WWW Document]. URL. https://www-sciencedirect-com.docelec.u-bordeaux.fr/science/

article/pii/0098300487900227 (accessed 4.22.19).
Hald, M., Steinsund, P.I., Korsun, S., Polyak, L., Aspeli, R., 1994. Recent and Late Quaternary distribution of *Elphidium excavatum* f. clavatum in Arctic seas. Cushman Found. Spec. Publ. 32, 53.
Jennings, A.E., Weiner, N.J., Helgadottir, G., Andrews, J.T., 2004. Modern foraminiferal faunas of the southwestern to northern Iceland shelf: oceanographic and environmental controls. J. Foraminifer. Res. 34, 180–207. https://doi.org/10.2113/34.3.180.
Jennings, A., Sheldon, C., Cronin, T., Francus, P., Stoner, J., Andrews, J., 2011. The Holocene history of Nares Strait: transition from Glacial Bay to Arctic-Atlantic throughflow. Oceanography 24, 26–41. https://doi.org/10.5670/oceanog.2011.52.
Jennings, A.E., Andrews, J.T., Ó Cofaigh, C., Onge, G.St., Sheldon, C., Belt, S.T., Cabedo-Sanz, P., Hillaire-Marcel, C., 2017. Ocean forcing of Ice Sheet retreat in central west Greenland from LGM to the early Holocene. Earth Planet. Sci. Lett. 472, 1–13. https://doi.org/10.1016/j.epsl.2017.05.007.
Jennings, A.E., Andrews, J.T., Oliver, B., Walczak, M., Mix, A., 2019. Retreat of the Smith Sound ice stream in the Early Holocene. Boreas 48, 825–840. https://doi.org/10.1111/bor.12391.
Jones, E.P., Eert, A.J., 2004. Waters of Nares Strait in 2001. Polarforschung 73, 185–189.
Juggins, S., 2019. rioja: Analysis of Quaternary Science Data.
Kanna, N., Sugiyama, S., Ohashi, Y., Sakakibara, D., Fukamachi, Y., Nomura, D., 2018. Upwelling of macronutrients and dissolved inorganic carbon by a subglacial freshwater driven plume in Bowdoin Fjord, Northwestern Greenland. J. Geophys. Res. Biogeosci. 123, 1666–1682. https://doi.org/10.1029/2017JG004248.
Knudsen, K.L., Stabell, B., Seidenkrantz, M.-S., Eiríksson, J., Blake, W., 2008. Deglacial and Holocene conditions in northernmost Baffin Bay: sediments, foraminifera, diatoms and stable isotopes. Boreas 37, 346–376. https://doi.org/10.1111/j.1502-3885.2008.00035.x.
Kozo, T.L., 1991. The hybrid polynya at the northern end of Nares Strait. Geophys. Res. Lett. 18, 2059–2062. https://doi.org/10.1029/91GL02574.
Krembs, C., Tuschling, K., Juterzenka, K., 2002. The topography of the ice-water interface – its influence on the colonization of sea ice by algae. Polar Biol. 25, 106–117. https://doi.org/10.1007/s003000100318.
Kwok, R., Untersteiner, N., 2011. The thinning of Arctic sea ice. Phys. Today 64, 36–41. https://doi.org/10.1063/1.3580491.
Kwok, R., Toudal Pedersen, L., Gudmandsen, P., Pang, S.S., 2010. Large sea ice outflow into the Nares Strait in 2007: Nares Strait sea ice outflow. Geophys. Res. Lett. 37 n/a-n/a. https://doi.org/10.1029/2009GL041872.
Lecavalier, B.S., Milne, G.A., Simpson, M.J.R., Wake, L., Huybrechts, P., Tarasov, L., Kjeldsen, K.K., Funder, S., Long, A.J., Woodroffe, S., Dyke, A.S., Larsen, N.K., 2014. A model of Greenland ice sheet deglaciation constrained by observations of relative sea level and ice extent. Quat. Sci. Rev. 102, 54–84. https://doi.org/10.1016/j.quascirev.2014.07.018.
Lecavalier, B.S., Fisher, D.A., Milne, G.A., Vinther, B.M., Tarasov, L., Huybrechts, P., Lacelle, D., Main, B., Zheng, J., Bourgeois, J., Dyke, A.S., 2017. High Arctic Holocene temperature record from the Agassiz ice cap and Greenland ice sheet evolution. Proc. Natl. Acad. Sci. 201616287. https://doi.org/10.1073/pnas.1616287114.
Marchese, C., Albouy, C., Tremblay, J.-É., Dumont, D., D'Ortenzio, F., Vissault, S., Bélanger, S., 2017. Changes in phytoplankton bloom phenology over the North Water (NOW) polynya: a response to changing environmental conditions. Polar Biol. 40, 1721–1737. https://doi.org/10.1007/s00300-017-2095-2.
Mayot, N., Matrai, P., Ellingsen, I.H., Steele, M., Johnson, K., Riser, S.C., Swift, D., 2018. Assessing phytoplankton activities in the seasonal ice zone of the Greenland Sea over an annual cycle. J. Geophys. Res. Oceans 123, 8004–8025. https://doi.org/10.1029/2018JC014271.
McGeehan, T., Maslowski, W., 2012. Evaluation and control mechanisms of volume and freshwater export through the Canadian Arctic Archipelago in a high-resolution pan-Arctic ice-ocean model: Canadian archipelago throughflow. J. Geophys. Res. Oceans 117 n/a-n/a. https://doi.org/10.1029/2011JC007261.
Melling, H., Gratton, Y., Ingram, G., 2001. Ocean circulation within the North Water polynya of Baffin Bay. Atmosphere-Ocean 39, 301–325. https://doi.org/10.1080/07055900.2001.9649683.
Moore, G.W.K., McNeil, K., 2018. The early collapse of the 2017 Lincoln Sea ice arch in response to anomalous sea ice and wind forcing. Geophys. Res. Lett. 45, 8343–8351. https://doi.org/10.1029/2018GL078428.
Münchow, A., 2016. Volume and freshwater flux observations from Nares Strait to the west of Greenland at daily time scales from 2003 to 2009. J. Phys. Oceanogr. 46, 141–157. https://doi.org/10.1175/JPO-D-15-0093.1.
Münchow, A., Melling, H., 2008. Ocean current observations from Nares Strait to the west of Greenland: Interannual to tidal variability and forcing. J. Mar. Res. 66, 801–833. https://doi.org/10.1357/002224008788064612.
Münchow, A., Falkner, K.K., Melling, H., 2007. Spatial continuity of measured seawater and tracer fluxes through Nares Strait, a dynamically wide channel bordering the Canadian Archipelago. J. Mar. Res. 65, 759–788. https://doi.org/10.1357/002224007784219048.
Münchow, A., Falkner, K.K., Melling, H., Rabe, B., Johnson, H.L., 2011. Ocean Warming and Freshening of Nares Strait Bottom Waters off NW Greenland 2003-09 14.
Nutt, D.C., 1966. The Drift of ice island WH-5. Arctic 19, 244–262. https://doi.org/10.14430/arctic3432.
Oksanen, J., Blanchet, F.G., Friendly, M., Kindt, R., Legendre, P., McGlinn, D., Minchin, P.R., O'Hara, R.B., Simpson, G.L., Solymos, P., Stevens, M.H.H., Szoecs, E., Wagner, H., 2019. Vegan: Community Ecology Package.
Polyak, L., Korsun, S., Febo, L.A., Stanovoy, V., Khusid, T., Hald, M., Paulsen, B.E., Lubinski, D.J., 2002. Benthic foraminiferal assemblages from the southern Kara Sea, a river-influenced arctic marine environment. J. Foraminifer. Res. 32, 252–273. https://doi.org/10.2113/32.3.252.
Racine, C., 2019. Ecologie des foraminifères benthiques en domaine arctique dans un contexte de changement climatique: cas des mer de Chukchi. (Barents et Baffin).
R Core Team, 2017. R: A language and environment for statistical computing. R Foundation for Statistical Computing, Vienna, Austria. https://www.R-project.org/.
Reusche, M.M., Marcott, S.A., Ceperley, E.G., Barth, A.M., Brook, E.J., Mix, A.C., Caffee, M.W., 2018. Early to Late Holocene surface exposure ages from two marine-terminating outlet glaciers in northwest Greenland. Geophys. Res. Lett. 45, 7028–7039. https://doi.org/10.1029/2018GL078266.
Ribeiro, S., Sejr, M.K., Limoges, A., Heikkilä, M., Andersen, T.J., Tallberg, P., Weckström, K., Husum, K., Forwick, M., Dalsgaard, T., Massé, G., Seidenkrantz, M.-S., Rysgaard, S., 2017. Sea ice and primary production proxies in surface sediments from a High Arctic Greenland fjord: Spatial distribution and implications for palaeoenvironmental studies. Ambio 46, 106–118. https://doi.org/10.1007/s13280-016-0894-2.
Rigor, I.G., Wallace, J.M., Colony, R.L., 2002. Response of sea ice to the Arctic oscillation. J. Clim. 15, 2648–2663. https://doi.org/10.1175/1520-0442(2002)015<2648:ROSITT>2.0.CO;2.
Rytter, F., Knudsen, K.L., Seidenkrantz, M.-S., Eiríksson, J., 2002. Modern distribution of benthic foraminifera on the North Icelandic shelf and slope. J. Foraminifer. Res. 32, 217–244. https://doi.org/10.2113/32.3.217.
Sadler, H.E., 1976. Water, heat, and salt transports through Nares Strait, Ellesmere Island. J. Fish. Res. Board Can. 33, 2286–2295. https://doi.org/10.1139/f76-275.
Samelson, R.M., Barbour, P.L., 2008. Low-level jets, orographic effects, and extreme events in Nares Strait: a model-based mesoscale climatology. Mon. Weather Rev. 136, 4746–4759. https://doi.org/10.1175/2007MWR2326.1.
Shadwick, E.H., Rintoul, S.R., Tilbrook, B., Williams, G.D., Young, N., Fraser, A.D., Marchant, H., Smith, J., Tamura, T., 2013. Glacier tongue calving reduced dense water formation and enhanced carbon uptake: ocean changes following glacier calving. Geophys. Res. Lett. 40, 904–909. https://doi.org/10.1002/grl.50178.
Smedsrud, L.H., Esau, I., Ingvaldsen, R.B., Eldevik, T., Haugan, P.M., Li, C., Lien, V.S., Olsen, A., Omar, A.M., Otterå, O.H., Risebrobakken, B., Sandø, A.B., Semenov, V.A., Sorokina, S.A., 2013. The role of the Barents Sea in the Arctic climate system. Rev. Geophys. 51, 415–449. https://doi.org/10.1002/rog.20017.
Sperling, M., Weldeab, S., Schmiedl, G., 2002. Drying of samples may alter foraminiferal isotopic ratios and faunistic composition. Micropaleontology 48, 87–91. https://doi.org/10.1661/0026-2803(2002)048[0087:DOSMAF]2.0.CO;2.
Steele, M., Morison, J., Ermold, W., Rigor, I., Ortmeyer, M., Shimada, K., 2004. Circulation of summer Pacific halocline water in the Arctic Ocean. J. Geophys. Res. Oceans 109. https://doi.org/10.1029/2003JC002009.
Steinsund, P.I., Hald, M., 1994. Recent calcium carbonate dissolution in the Barents Sea: paleoceanographic applications. Mar. Geol. 117, 303–316. https://doi.org/10.1016/0025-3227(94)90022-1.
Vilks, G., 1969. Recent foraminifera in the Canadian Arctic. Micropaleontology 15, 35–60. https://doi.org/10.2307/1484859.
Wang, J., Zhang, J., Watanabe, E., Ikeda, M., Mizobata, K., Walsh, J.E., Bai, X., Wu, B., 2009. Is the Dipole Anomaly a major driver to record lows in Arctic summer sea ice extent? Geophys. Res. Lett. 36. https://doi.org/10.1029/2008GL036706.
Wood, S., 2019. mgcv: Mixed GAM Computation Vehicle With Automatic Smoothness Estimation.